Measurement of the scintillation yield of low-energy electrons in liquid xenon

E. Aprile,[1] R. Budnik,[1] B. Choi,[1] H. A. Contreras,[1] K.-L. Giboni,[1] L. W. Goetzke,[1] J. E. Koglin,[1,*] R. F. Lang,[1,†] K. E. Lim,[1,‡] A. J. Melgarejo Fernandez,[1] R. Persiani,[2] G. Plante,[1] and A. Rizzo[1]

[1]*Physics Department, Columbia University, New York, New York 10027, USA*
[2]*University of Bologna and INFN-Bologna, Bologna, Italy*

(Received 18 September 2012; published 18 December 2012)

We have measured the energy dependence of the liquid xenon (LXe) scintillation yield of electrons with energies between 2.1 and 120.2 keV, using the Compton coincidence technique. A LXe scintillation detector with a very high light detection efficiency was irradiated with ^{137}Cs γ rays, and the energy of the Compton-scattered γ rays was measured with a high-purity germanium detector placed at different scattering angles. The excellent energy resolution of the high-purity germanium detector allows the selection of events with Compton electrons of known energy in the LXe detector. We find that the scintillation yield initially increases as the electron energy decreases from 120 to about 60 keV but then decreases by about 30% from 60 to 2 keV. The scintillation yield was also measured with conversion electrons from the 32.1 and 9.4 keV transitions of the ^{83m}Kr isomer, used as an internal calibration source. We find that the scintillation yield of the 32.1 keV transition is compatible with that obtained from the Compton coincidence measurement. On the other hand, the yield for the 9.4 keV transition is much higher than that measured for a Compton electron of the same energy. We interpret the enhancement in the scintillation yield as due to the enhanced recombination rate in the presence of Xe ions left from the 32.1 keV transition, which precedes the 9.4 keV one by 220 ns, on average.

DOI: 10.1103/PhysRevD.86.112004 PACS numbers: 78.70.−g, 14.80.Ly, 95.55.Vj

I. INTRODUCTION

The experimental work presented in this paper is part of an ongoing effort to understand the ionization and scintillation response of liquid xenon (LXe) to low energy (< 10 keV) particles, relevant to the interpretation of data from dark matter searches based on LXe, XENON100 in particular. Data from the current XENON100 experiment have resulted in the most stringent limits to the interaction cross section for a variety of dark matter weakly interacting massive particle masses [1–3]. The next generation experiment, XENON1T, should provide almost two orders of magnitude sensitivity improvement [4].

The XENON detectors are time projection chambers in which both the ionization, via proportional scintillation light, and the direct scintillation light produced by particle interactions in the sensitive LXe volume are recorded by photomultipliers (PMTs) [5]. The scintillation and ionization response of LXe depends on the electronic stopping power for the recoil type, its energy, and the strength of the applied electric field. The detector energy scale, for a given type of recoil, can in principle be constructed from the scintillation signal, the ionization signal, or a combination of both. Inferring the energy of the particle from the measured signals thus requires a precise knowledge of the response of LXe to low-energy nuclear recoils, produced by weakly interacting massive particles or background neutrons, and electronic recoils, produced by electromagnetic background. We have already reported several measurements of the relative scintillation efficiency of nuclear recoils in LXe [6–8], with the latest measurements giving the most precise values to date for this quantity and for recoil energies as low as 3 keV. The abundance of measurements of the relative scintillation efficiency of nuclear recoils, compared to the relatively few measurements of their ionization yield, is the reason why a scintillation-based energy scale is often chosen instead of an ionization-based or a ''combined'' energy scale. In this paper we present our first measurement of the scintillation yield of electronic recoils at zero electric field in the energy range of 2.1 to 120.2 keV.

A recoiling electron in LXe produces a track of ionized and excited Xe atoms or excitons. Both excitons and Xe ions that recombine with electrons lead to the formation of excited dimers which subsequently deexcite and produce scintillation photons. The ratio of the number of excitons to the number of ions produced, $N_{\mathrm{ex}}/N_{\mathrm{i}}$, is between 0.06 and 0.20 [9], and hence the contribution to the scintillation signal from direct excitation is small. If an electric field is applied, the fraction of scintillation light that originates from recombining electron-ion pairs is reduced. This fraction can thus be varied by changing the applied electric field. However, even at zero electric field, not all electrons recombine in a time scale practical for the collection of the scintillation photons produced [10]. In LXe, the nonlinearity in the scintillation signal from electronic recoils at

*Present address: SLAC National Accelerator Laboratory, Menlo Park, California 94025, USA.
†Present address: Physics Department, Purdue University, West Lafayette, Indiana 47907, USA.
‡Corresponding author. kelim@phys.columbia.edu

zero electric field is understood as being the result of the energy dependence of the recombination probability.

Measurements of the scintillation yield of electrons of low energy ($\lesssim 100$ keV) in LXe are scarce. At these energies, in most cases, scintillation light yield measurements have been carried out with monoenergetic sources [11–13], where photoelectric absorption is the dominant interaction. One disadvantage of using photoabsorbed γ rays to measure the scintillation yield is that multiple energetic electrons are produced as a result of the photoabsorption: a photoelectron with an energy $E_\gamma - E_b$, the incident γ-ray energy minus the electron binding energy, and a host of deexcitation Auger electrons or x rays photoabsorbed afterwards. The scintillation yield obtained is then the convolution of the distribution of electron energies produced with the scintillation response of LXe to electrons, instead of that of an electron of that energy. On the other hand, a γ-ray Compton scatter produces a single energetic electron with an energy very close to $E_\gamma - E'_\gamma$, the incident γ-ray energy minus the scattered γ-ray energy. This is because Compton scattering is essentially equally probable for all atomic electrons instead of only for those with significant binding energies, as is the case for photoelectric absorption. Furthermore, the low-energy electromagnetic background in a LXe dark matter detector is induced by Compton-scattered high-energy γ rays from the radioactivities present largely in construction materials and the environment. A second difficulty arising in measurements with external low-energy γ rays is the shallow penetration depth into the active volume of the LXe detector.

Measurements of the scintillation yield of low-energy electrons in LXe have also been performed via internal irradiation with conversion electrons from the ^{83m}Kr isomer [14,15]. Despite solving the problems of low-energy external sources, the extremely limited number of isotopes that can be used for such irradiations prevents the measurement of the scintillation yield over a continuous energy range.

The Compton coincidence technique, introduced by Valentine and Rooney [16,17] and further improved by Choong *et al.* [18], allows the measurement of the electron response of scintillators at low energies. This method uses the energetic electrons produced by Compton-scattered γ rays from a monoenergetic, high-energy source incident upon a scintillation detector. If a γ ray of energy E_γ scatters in the scintillator, exits with energy E'_γ, and does not interact anywhere else, the energy of the Compton electron produced, E_{er}, is given by

$$E_{\mathrm{er}} = E_\gamma - E'_\gamma, \tag{1}$$

$$= E_\gamma - \frac{E_\gamma}{1 + \frac{E_\gamma}{m_e c^2}(1 - \cos\theta)}, \tag{2}$$

where m_e is the electron mass, and θ is the scattering angle. By using a second detector in coincidence with the scintillation detector and measuring the energy of the scattered γ ray, it is possible to select nearly monoenergetic electronic recoils from the continuous spectrum of Compton electrons produced. By varying the angle at which the second detector is positioned and the range of scattered γ energies selected, one can choose the energy at which the electron response is measured.

The experimental setup is described in Sec. II, the calibration in Sec. III, the Compton coincidence measurements and data analysis in Sec. IV, and the response to monoenergetic γ sources in Sec. V. The results are presented in Sec. VI, followed by a discussion in Sec. VII.

II. EXPERIMENTAL SETUP

The measurement of the scintillation response of LXe to electronic recoils was performed by irradiating a LXe detector with γ rays from a 370 MBq ^{137}Cs source and measuring the energy of the scattered γ rays at various angles with a high-purity germanium (HPGe) detector. Figure 1 shows a schematic of the experimental setup. The energy deposit in the LXe is inferred from the energy measured in the HPGe detector, as expressed in Eq. (1). The angle at which the HPGe detector is positioned, θ_{HPGe}, is adjusted to produce recoils in the desired energy range.

The LXe detector was designed with minimal materials outside of the active volume to reduce the γ-ray scattering probability before and after an interaction in the active volume. The active volume is a cube of side length 2.6 cm covered by six 2.5 cm square Hamamatsu R8520-406-SEL PMTs mounted in a polytetrafluoroethylene (PTFE) frame. The PMTs are the same type as those

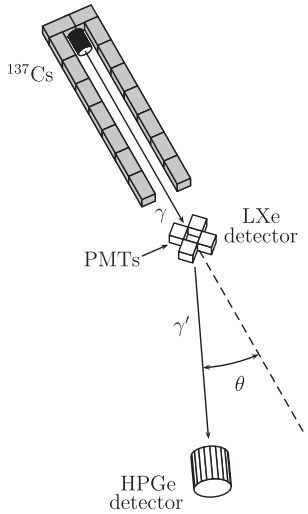

FIG. 1. Schematic of the experimental setup. A 370 MBq ^{137}Cs source is placed 85 cm from a LXe target viewed by six PMTs (only four shown, top and bottom PMTs are omitted for clarity). The energy of the γ rays that scatter near an angle θ_{HPGe} are measured with a HPGe detector. The excellent energy resolution of the HPGe detector allows the selection of events where a Compton electron of the desired energy is produced in the LXe detector.

used in the XENON100 experiment [2] but selected for high quantum efficiency (QE). They have a bialkali photocathode designed for low-temperature operation down to $-110\,^{\circ}$C and an average room temperature QE of 32% at 178 nm, the wavelength at which Xe scintillates [19]. The measured QE values were provided by Hamamatsu. The high QE of the PMTs and the large photocathode coverage of the arrangement yields a very high light collection efficiency and thus enables a low-energy threshold. The PMTs were biased with positive high voltage to keep the PMT metal body and photocathode at ground potential, thereby ensuring that no electric field is present in the LXe active volume. More details on the LXe detector can be found in Ref. [8].

The LXe detector vessel was filled with 1.82 kg of LXe, the amount required for the liquid level to reach 1 cm above the active volume. The total LXe mass in the active volume is 50 g. During operation, the Xe is purified in the gas phase by circulating it through a hot getter with a diaphragm pump. The purified gas is reliquefied efficiently using a heat exchanger [20]. The LXe temperature is kept constant with an Iwatani PDC08 pulse tube refrigerator delivering 24 W of cooling power at $-106\,^{\circ}$C. More details on the cooling system for this experiment are given in Ref. [20]. For the measurements presented here, the LXe temperature was maintained at $-95\,^{\circ}$C, which corresponds to a vapor pressure of 2 atm. The LXe detector operating conditions were stable throughout the entire data-taking period, with observed LXe temperature and gaseous xenon pressure variations (standard deviation over mean) of less than 0.7 and 0.6%, respectively.

The Compton-scattered γ rays were tagged with an ORTEC p-type coaxial HPGe detector of 5.8-cm diameter and 4.8-cm depth. The typical full width at half maximum energy resolution at 1.33 MeV and the peak-to-Compton ratio are specified by ORTEC to be less than 2.09 keV and better than 51:1, respectively.

The ^{137}Cs source was aligned with respect to the center of the LXe detector active volume using an autoleveling laser. The desired HPGe detector floor positions were measured with a 1.5-m aluminium rule and a plumb line. The vertical position of the HPGe detector was set with the laser. The location of the ^{137}Cs source was fixed at distance of 85 cm from the center of the active volume of the LXe detector. Lead bricks lined the path between the source and the LXe detector to minimize the scattering of γ rays outside the active volume of the LXe detector. The distance between the LXe detector and the HPGe detector was varied from 14 to 62 cm (see Table I). The uncertainty in the position of the HPGe detector was estimated to be less than 3 mm.

The signals from the six PMTs were fed into a Phillips 776×10 amplifier with two amplified outputs per channel. The first output of each channel was digitized by a 14-bit CAEN V1724 100 MS/s flash analog-to-digital converter (ADC) with 40 MHz bandwidth, while the second output was fed to a Phillips 706 leading edge discriminator. The discriminator thresholds were set at a level of -20 mV, which corresponds to 0.7 photoelectrons (pe). The logic signals of the six discriminator outputs were added with a CAEN N401 linear fan-in and discriminated to obtain a twofold PMT coincidence condition. The twofold PMT coincidence logic signal was then passed to a 10 μs hold-off circuit to prevent retriggering on the tail of the LXe scintillation signal, and constituted the LXe trigger.

TABLE I. HPGe detector positions, measured full absorption peak energy resolutions, and selected electronic recoil energy ranges for all Compton coincidence data sets. The variation of the measured resolution is discussed in Sec. III B.

θ_{HPGe}	HPGe Detector Distance (cm)	HPGe Detector Resolution (keV)	E_{er} Range (keV)
0°	14	1.4	2.2–26.5
5.6°	60	1.0	2.0–12.9
8.6°	40	1.0	5.1–28.8
12.0°	40	1.0	10.0–27.2
16.1°	62	1.3	21.8–36.2
21.3°	40	1.0	33.9–60.2
28.1°	40	1.1	63.2–90.2
34.4°	19	1.7	77.2–122.2
34.4°	40	1.0	112.2–114.2

The signal of the HPGe detector was amplified with an ORTEC A257N preamplifier and shaped with an ORTEC 450 research amplifier using 1 and 0.5 μs differentiation and integration time constants, respectively. The output of the research amplifier was split with a passive resistive fan-out. One copy went directly to the flash ADC and the other copy was discriminated at a threshold level of -30 mV, to form the HPGe trigger signal.

Finally, for the Compton coincidence measurements presented here, the trigger was given by the coincidence within a 200-ns window of the LXe and the HPGe trigger signals.

The energy dependence of the efficiency of the LXe trigger was measured using a ^{22}Na source and a NaI(Tl) detector with the technique described in Ref. [8]. The result obtained was compatible with the measurement of Ref. [8], confirming that recoil energy spectra do not suffer efficiency losses in the energy region of interest. For some of the data sets taken at higher energies ($\theta_{\mathrm{HPGe}} = 8.6°$, 16.1°), the threshold levels were set to -40 mV so as to reduce the fraction of noise triggers. These increased thresholds also did not decrease the event acceptance in the energy region of interest.

III. CALIBRATION

A. LXe detector calibration

A blue light emitting diode (LED) embedded in the PTFE mounting structure was used to calibrate the gain

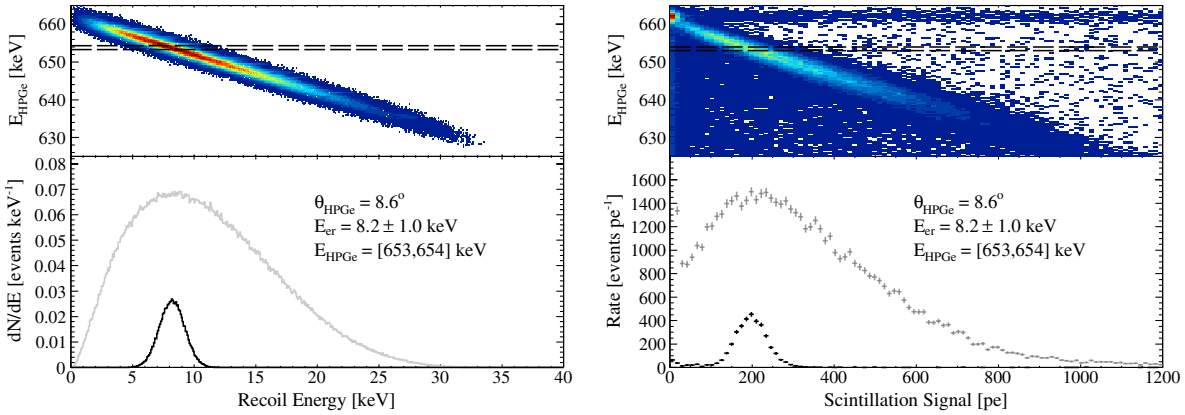

FIG. 2 (color online). Simulated (left, top) and measured (right, top) distributions of HPGe detector energies and Compton electron recoil energies, or LXe scintillation signals in the case of the measurement, along with their projections (bottom, gray points) for the 8.6° Compton coincidence setup. A known electronic recoil energy spectrum (black points) is obtained by selecting simulated events with HPGe detector energies between 653 and 654 keV (horizontal dashed lines). With this energy selection, the spread in electronic recoil energies is dominated by the HPGe detector energy resolution of 1 keV at 661.7 keV measured for this dataset (Sec. III B). Using the same energy selection (horizontal dashed lines), the scintillation response of LXe to 8.2 keV electronic recoils can be extracted from the 8.6° Compton coincidence measurement. Additional backgrounds, neglected in the simulation, are present in the data. They become important only at recoil energies below 5 keV, as explained in the text.

of each PMT. The light level from the LED was adjusted such that the contamination of the single-photoelectron peak from the double-photoelectron peak was negligible. The gain value for each LED data set was determined by fitting both the single-photoelectron peak and the noise pedestal with Gaussian functions. The gain was taken as the difference between the means of each Gaussian. The PMT gain calibration was performed at regular intervals during data taking. For the analysis presented here, the gain of each PMT was taken as their average measured gain over the whole data-taking period and its uncertainty as the variation in the individual gain measurements. The uncertainty in the gain of each PMT varied between 1 and 1.6%. Since the total scintillation signal is obtained from the sum of all PMT signals, this leads to a total contribution to the uncertainty on the measured scintillation signal of 3%.

B. HPGe detector calibration

The excellent energy resolution of the HPGe detector makes it possible to select events where γ rays Compton scatter once and deposit a fixed energy in the LXe detector. Since the energy of the electronic recoil in the LXe detector is directly determined by the measured energy in the HPGe detector, it is important to verify the stability of the HPGe detector response throughout the measurements.

The HPGe detector was calibrated through dedicated measurements with the ^{137}Cs source between each Compton coincidence measurement. The linearity of the energy calibration was verified with 511 keV γ rays from a ^{22}Na source.

In addition, the stability of the HPGe detector calibration was monitored during each Compton coincidence measurement via accidental coincidence events. Accidental coincidence events from uncorrelated LXe and HPGe triggers occur when two different γ rays interact in the LXe detector and the HPGe detector within the 200-ns coincidence window time. Since the accidental coincidence HPGe energy spectrum is essentially the same, albeit with a smaller rate, as an energy spectrum taken with the HPGe trigger, the 661.7 keV full absorption peak from ^{137}Cs γ rays incident on the HPGe detector can thus be used to monitor the stability of the calibration [see Fig. 2 (right)]. The HPGe detector calibration factor was also corrected for adjustments of the dc offset of the HPGe channel of the flash ADC. For the Compton coincidence measurements presented here, the maximum variation in the corrected HPGe calibration factor was 0.2%. The energy resolution at 661.7 keV, obtained via accidental coincidence events, varied between 1.0 and 1.7 keV (see Table I). This variation is attributed to long-term changes (< 0.5 mV) in the baseline of the HPGe channel. The effect of these small baseline changes could have been eliminated by optimizing the amplifier gain to use the full dynamic range of the flash ADC.

IV. COMPTON COINCIDENCE MEASUREMENTS

A. Measured electronic recoil distributions

Compton coincidence data sets were taken with the HPGe detector positioned at eight different scattering angles, θ_{HPGe}: 0°, 5.6°, 8.6°, 12.0°, 16.1°, 21.3°, 28.1°, and 34.4°, with LXe and HPGe detector distances varying between 14 and 62 cm, resulting in electronic recoil spectra with energies ranging from 2.0 to 122.2 keV. At each angle, a range of electronic recoil energies are deposited in the LXe detector due to the angular acceptance of the LXe

target and that of the HPGe detector. Therefore, the HPGe detector positions were chosen so as to obtain recoil energies covering the above energy range with sufficient statistics. Table I lists the HPGe detector positions used for each angle. In addition, a second 34.4° data set was taken with a different LXe and HPGe detector distance to investigate a possible systematic effect on the measured scintillation yield from the HPGe detector position. Finally, two data sets with different trigger configurations were taken at 0° to help study background contributions at recoil energies below 5 keV, one with a LXe detector trigger only, and one with a HPGe detector trigger only.

Since electronic recoils with a range of energies are accessible in one measurement with the HPGe detector at a given position, and since the energy resolution of the HPGe detector is much narrower than this energy range, the scintillation response at many different recoil energies can be extracted from a single data set. Moreover, the scintillation response at the same energy can be extracted from data sets which have overlapping recoil energy ranges.

The distribution of HPGe detector energies, E_{HPGe}, and Compton electron recoil energies in the LXe detector, E_{er}, for the 8.6° Compton coincidence setup are shown in Fig. 2, for both data (right panel) and a simplified Monte Carlo simulation (left panel). The distribution of energy deposits in both detectors is shown in the top panel, while the bottom one shows only the depositions in the LXe detector (gray line). This simplified simulation, described in Sec. IV B, only includes γ-ray interactions with the detector targets, ignoring all other materials, and takes into account the energy resolution of the HPGe detector. As expected, the energy of the scattered γ ray and that of the recoiling Compton electron sum up to the energy of the γ-ray incident on the LXe detector, E_γ. Recoils over a range of energies are produced in the LXe detector due to the angular acceptance of both detectors, as expected. A distribution of known electronic recoil energies (black line in the bottom panel) can be obtained by selecting a narrow range of scattered γ-ray energies (horizontal dashed lines) measured by the HPGe detector. The spread in electronic recoil energies after the selection is given by the convolution of the energy range chosen, ΔE_{HPGe}, with the HPGe detector resolution near E_γ. The scintillation response at a given electronic recoil energy is obtained by calculating the mean scintillation signal measured in the LXe detector when applying this HPGe detector energy selection.

Figure 2 (right, top), shows the measured distribution of HPGe detector energies and LXe detector scintillation signals for the 8.6° Compton coincidence data set. Comparing this with the distribution from the simulated data, three different event populations are visible: events with $E_{\mathrm{er}} + E_{\mathrm{HPGe}}$ equal, lower, and higher than E_γ. The event population where $E_{\mathrm{er}} + E_{\mathrm{HPGe}} = E_\gamma$, within the limits of the HPGe detector resolution, corresponds to events where the incident γ ray scatters once in the active LXe volume, producing a Compton electron of energy E_{er}, and is fully absorbed in the HPGe detector. Consequently, the scintillation response of LXe to nearly monoenergetic electronic recoils can be inferred from these events.

The event population where $E_{\mathrm{er}} + E_{\mathrm{HPGe}}$ is lower than E_γ corresponds, for the most part, to events where the scattered γ ray deposits only a fraction of its energy in the HPGe detector, due to the finite size of the crystal. That is, each possible scattered γ-ray energy is responsible for a spectrum of energies in the HPGe detector, with a full absorption peak, a Compton continuum, a multiple Compton scattering region, the latter two being responsible for the event population with E_{HPGe} lower than the scattered γ-ray energy. Events where γ rays scatter in other materials before interacting in the HPGe detector additionally contribute to this population. A Monte Carlo simulation based on the GEANT4 toolkit [21], also described in Sec. IV B, was used to estimate the contribution of such events in the energy range of the single scatter peak for various electronic recoil spectra.

Finally, the event population where $E_{\mathrm{er}} + E_{\mathrm{HPGe}}$ is higher than E_γ corresponds to events with an accidental coincidence between the LXe detector and the HPGe detector. This population is especially pronounced at $E_{\mathrm{HPGe}} \approx 662$ keV in Fig. 2 (right), as expected since the accidental coincidence spectrum should have a peak at the incident γ-ray energy. As mentioned in Sec. III B, events from this population were used to monitor the stability of the HPGe energy calibration during the Compton coincidence measurements.

The increase in rate at low recoil energies compared to the simulated data is attributed to events where the γ ray interacts only in the LXe outside the active volume but where the resulting scintillation light is visible in the active volume. The feature is also observed with all external γ-ray sources. The average probability for a photon outside the active LXe volume to reach a PMT photocathode was estimated at 1×10^{-4} via a light propagation Monte Carlo simulation. An exponential feature consistent with that observed in the data can also be reproduced in simulations by including the expected scintillation signal from energy deposits outside the active LXe volume. As is apparent from Fig. 2 (right, top), the largest background in the measurement of the scintillation response of LXe with this technique is from accidental coincidences at low electronic recoil energies.

B. Monte Carlo simulation

For optimum efficiency, two different Monte Carlo simulations were used to analyze different aspects of the expected event distributions for Compton coincidence measurements. The first is a simplified Monte Carlo simulation that considers only events in which the incident γ ray interacts in the LXe detector and deposits its full

energy in the HPGe detector. The second simulation is based on the GEANT4 toolkit and includes a realistic description of the LXe detector, detector vessel, vacuum cryostat, support frame, and HPGe detector. It was used to obtain the expected electronic recoil energy spectra as a function of HPGe energy and thus enabled a direct comparison with the measured spectra and the identification and quantification of the different backgrounds present.

The simplified Monte Carlo simulation incorporates the geometry of the active LXe volume and of the HPGe detector crystal, the position of the ^{137}Cs source, as well as the actual positions of the HPGe detector used for the various Compton coincidence data sets. The simulation proceeds by generating random positions within the volume of the LXe detector, taking into account the Compton scattering mean free path, and on the front surface of the HPGe detector, and then calculating the recoil energy that corresponds to each pair of random LXe and HPGe interaction points via the Compton scattering formula. The energy deposited in the HPGe detector is then simply taken as the incident γ-ray energy, E_γ, minus the recoil energy in the LXe detector, thus assuming that the scattered γ ray deposited its full energy in the HPGe detector. This is then convolved with a Gaussian energy resolution. The standard deviation used for each Compton coincidence data set is the value measured using the corresponding accidental coincidence spectrum (see Sec. III B). Calculating the expected recoil energy from this simulation assumes that the incident γ ray travels directly from the source to the LXe detector, scatters once in the LXe detector, and travels directly to the HPGe detector, thereby neglecting any interactions in materials outside of the LXe active volume. Furthermore, since scattering angles are not sampled from the photon differential scattering cross section, the calculation neglects any angular dependence in the cross section over the range of scattering angles geometrically allowed by both detectors. Nevertheless, the expected mean energy of the recoil peak from the simplified simulation was found to be in agreement at the 1% level with that of the GEANT4-based simulation. In addition, the simulated spectra agree with each other at all recoil energies above 2 keV. Disagreement on the order of 10% appears for the 2-keV recoil peak below 1 keV.

As mentioned earlier, the resulting mean and spread of the electronic recoil peak in the LXe detector, for each HPGe energy selection window applied to a Compton coincidence data set, were calculated using the simplified simulation by applying the appropriate energy selections to each simulated data set. The effect of the misalignment of the HPGe detector on the mean energy of the recoil peak was investigated by varying the position of the HPGe detector in the simulation. Mean recoil energies were found to vary by less than 2%. Finally, the change in the response of the LXe detector due to the variation of the spatial event distribution in the LXe with the HPGe energy selection was estimated by calculating the average light detection efficiency over the spatial distribution of events for different HPGe energy selections. The spatial variation of the light detection efficiency used for the calculation was obtained from an independent light propagation Monte Carlo simulation. This simulation takes into account the geometry of the PMTs and the PTFE holding structure, the reflectivity of the materials in contact with the active LXe volume, the QE and collection efficiency of the PMTs, and an estimate of the angular response of the PMTs [22].

The GEANT4-based Monte Carlo simulation uses the same description of the LXe detector as the one used to simulate the expected nuclear recoil energy distributions for the measurement of the scintillation efficiency of low-energy nuclear recoils in LXe that was performed with the same detector [8]. The geometry and response of the HPGe detector was verified by comparing simulated energy spectra with measured spectra from dedicated ^{137}Cs calibrations of the HPGe detector. The information recorded in the simulation includes the energy, position, time, type of particle and physical process responsible for each energy deposit in the LXe detector, as well as the total energy, time, and type of particle for each energy deposit in the HPGe detector.

Figure 3 shows the simulated electronic recoil energy spectra for the 0° Compton coincidence setup, obtained from the GEANT4-based simulation using E_{HPGe} energy selections [659,660], [658,659], [657,658], and [656,657] keV, resulting in mean recoil energies of 2.2 ± 1.4, 3.2 ± 1.4, 4.2 ± 1.4, and 5.3 ± 1.4 keV, respectively. The black spectra consist of events in which the γ scattered only in the active LXe volume before interacting in the HPGe detector whereas the red spectra consist of events in which the γ ray additionally interacted in other materials, either before or after scattering in the active LXe volume, before interacting in the HPGe detector. The contribution of these multiple scatter events to the electronic recoil peak is less than 3%. Their energy spectrum is not peaked since the presence of additional scatters spoils the HPGe energy and LXe recoil energy correlation. Note, however, that since the selection is for a fixed HPGe energy, the maximum recoil energy for these events is constrained to be lower than the maximum energy of the recoil peak. Multiple scatters in the active LXe volume are highly suppressed due to the small size of the target with respect to the Compton scattering mean free path in LXe for ^{137}Cs γ rays (~ 5.5 cm). These spectra can be compared to the measured LXe scintillation spectra shown in Fig. 4, keeping in mind that the background contribution from accidental coincidence events is not included in the simulation. At energies of 3.2 keV and above, the measured electronic recoil peak is well separated from the background from accidental coincidences. This low contamination from events with scatters in other materials shows that the design

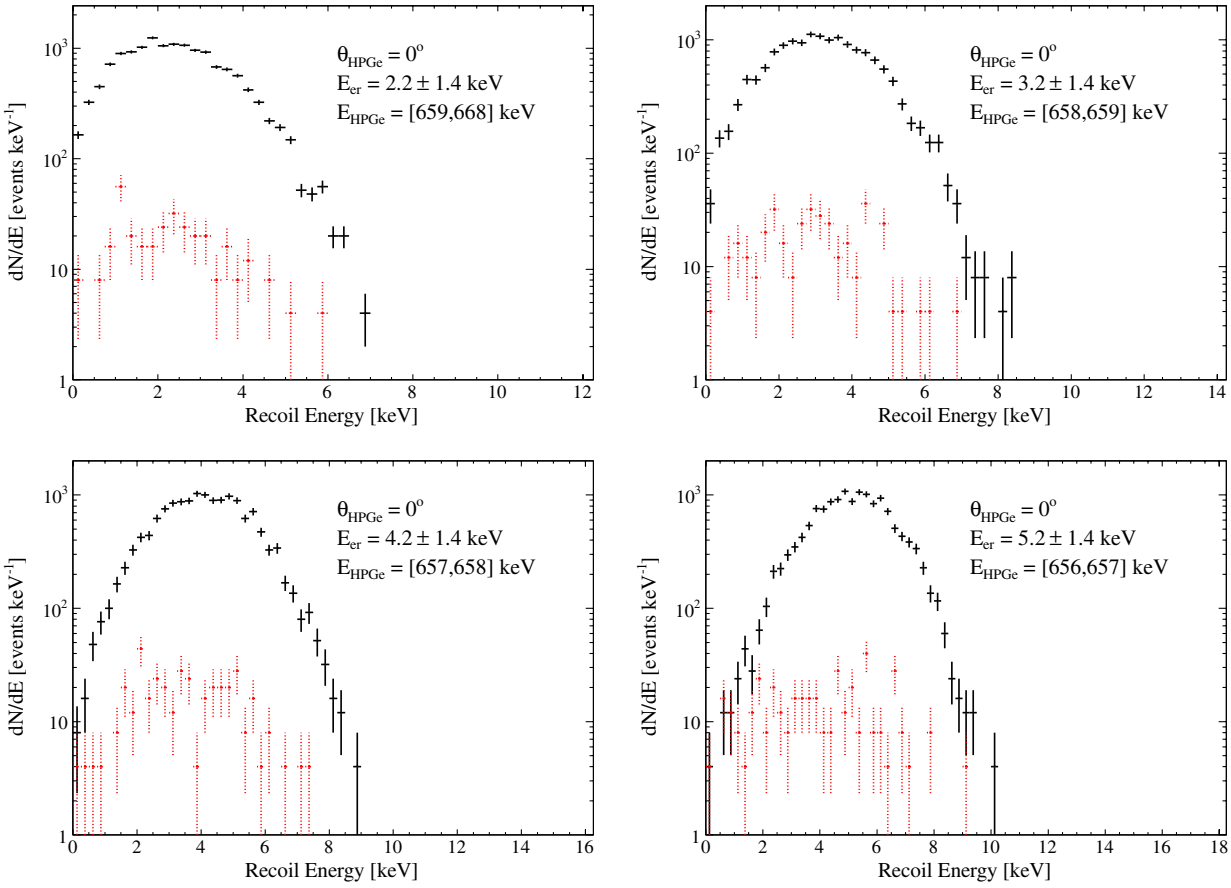

FIG. 3 (color online). Simulated electronic recoil energy spectra for the 0° Compton coincidence setup, using E_{HPGe} energy selections [659,660], [658,659], [657,658], and [656,657] keV, resulting in mean recoil energies of 2.2 ± 1.4, 3.2 ± 1.4, 4.2 ± 1.4 and 5.3 ± 1.4 keV, respectively. The black histograms show the spectrum of events where the incident γ ray interacts in the active LXe volume, and nowhere else, and deposits in the HPGe detector an energy within the HPGe selection window. The red dashed histograms correspond to events where the γ ray additionally interacts in other materials, either before or after scattering in the active LXe volume, before interacting in the HPGe detector. The contamination of the recoil peak by events with γ-ray interactions in other materials is less than 3%.

goal of minimizing the amount of materials in the vicinity of the active LXe volume has been achieved, in agreement with Ref. [8].

The electronic recoil spectra with mean recoil energies of 2.2 ± 1.4, 3.2 ± 1.4, 4.2 ± 1.4 keV were also used to calculate the uncertainty in the LXe scintillation response at low energies arising from the assumption of an exponential background model (Sec. IV C). The details of the calculation are described in Sec. VI.

C. The scintillation yield

For each scattering angle (θ_{HPGe}) at which Compton coincidence measurements were taken, the distribution of HPGe detector energies and LXe scintillation signals were divided in 1-keV slices along the E_{HPGe} axis, and the resulting LXe scintillation spectra were analyzed for each of the selected energies.

Figure 4 shows the LXe scintillation spectra obtained for the four lowest electronic recoil energies from the 0° Compton coincidence data set. For recoil energies below 2 keV, the background in the signal region is too high to extract the scintillation yield in LXe. The spectra consist of a recoil peak, which corresponds to events where the incident γ ray scattered in the active LXe volume only and deposited its full energy in the HPGe detector, and different backgrounds depending on the electronic recoil energy range selected. For spectra at low recoil energies, the background mostly comes from accidental coincidence events from the full absorption peak of ^{137}Cs in the HPGe detector and few photoelectrons scintillation signals from the LXe detector, believed to originate from interactions in the LXe outside the active volume, as discussed earlier. For spectra at recoil energies above 5 keV, the background largely comes from events in which scattered γ rays with energies higher than that expected for the HPGe energy selection deposit only a fraction of their energy in the HPGe detector, resulting in an approximately flat background from zero to the recoil peak. Ultimately, spectra at recoil energies above or below the range of energies

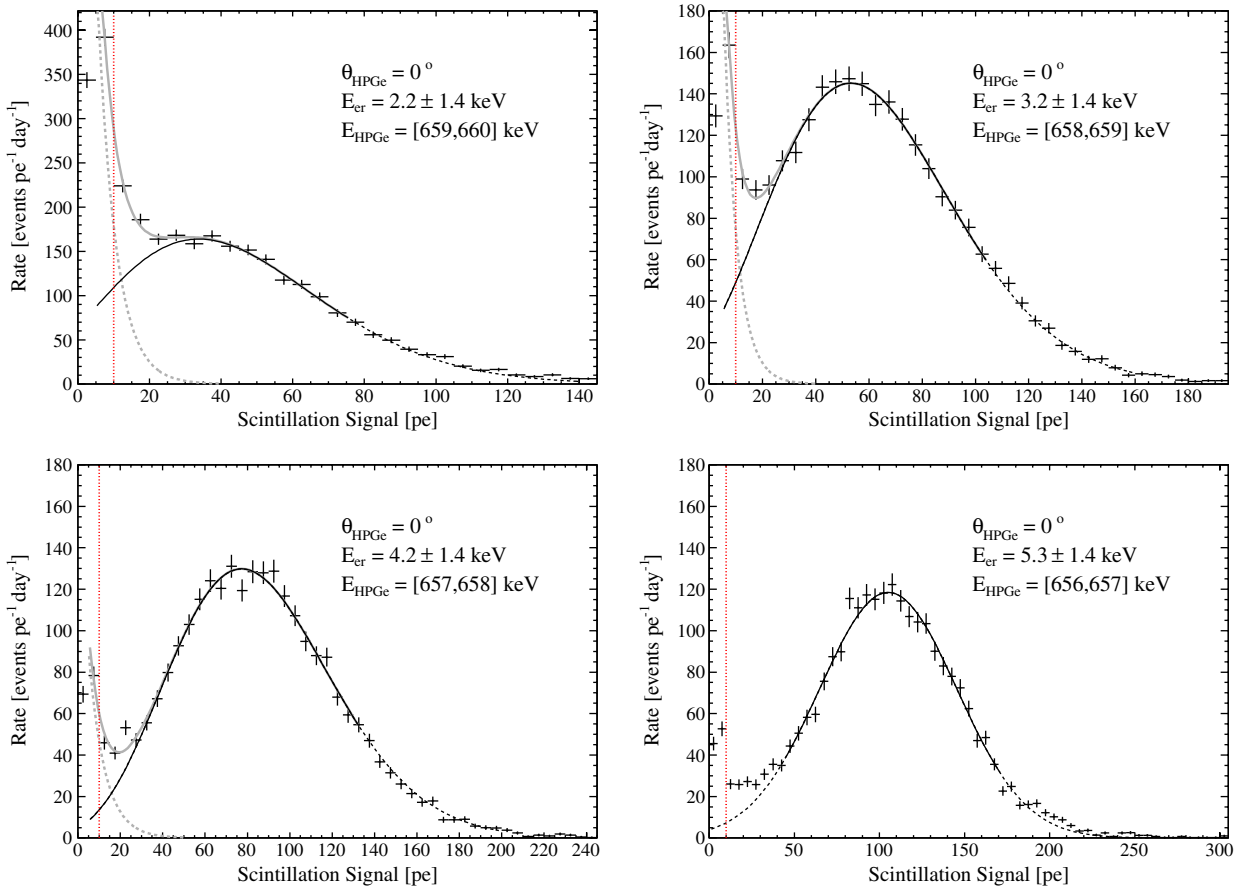

FIG. 4 (color online). LXe scintillation spectra (points) for electronic recoil energies of 2.2 ± 1.4, 3.2 ± 1.4, 4.2 ± 1.4, and 5.3 ± 1.4 keV from the 0° Compton coincidence data set with the same HPGe energy selection windows used in the Monte Carlo analysis. As a reference, the measured >99% trigger efficiency is indicated by the vertical red dashed line. For recoil energies E_{er} below 5 keV, the scintillation spectra were fitted with the sum (gray line) of a "scaled" continuous Poisson function (black line) and an exponential function (dashed gray line), as described in the text. The range used for each fit is indicated by the extent of the solid black line. For recoil energies above 5 keV, the spectra were fitted with Gaussian functions (black line).

expected from the angular acceptance of the LXe and HPGe detectors are dominated by events where the γ ray scattered in other materials and by accidental coincidence events between a partial energy deposit in both detectors.

For spectra at recoil energies below 5 keV, the recoil peaks are slightly asymmetric, exhibiting a longer tail at higher energies. Additionally, the background from accidental coincidence events is significant and must be taken into account to obtain the correct LXe scintillation response. Consequently, the spectra were fitted with the sum of a "scaled" continuous Poisson function, that is, a function of the form $f_{\mu,a}(x) = e^{-\mu}\mu^{ax}/\Gamma(ax+1)$, which describes the asymmetry of the recoil peak with the scaling parameter a, and an exponential function, which represents the background coming from accidental coincidence events. Figure 4 (top left, top right, bottom left) shows the results of fits to spectra at electronic recoil energies of 2.2 ± 1.4, 3.2 ± 1.4, and 4.2 ± 1.4 keV from the 0° Compton coincidence data set, respectively. Note that the uncertainty on the electronic recoil energy stated here (and throughout) corresponds to the spread in recoil energies after the HPGe energy selection (see Fig. 4 left), which is dominated by the HPGe energy resolution, and not the uncertainty on the mean energy of the recoil peak, which is considerably smaller.

For spectra at recoil energies above 5 keV, the recoil peaks are symmetric and the fraction of events arising from the background is small. Hence, these spectra were fitted with Gaussian functions over the range of the recoil peaks. Fig. 4 (bottom right) shows the result at 5.3 ± 1.4 keV from the 0° Compton coincidence data set. The background from scattered γ rays with partial energy deposited in the HPGe detector is apparent to the left of the recoil peak.

As explained in Sec. IVA, each Compton coincidence data set can be used to infer the scintillation response over a wide range of energies, limited mostly by the angular acceptance of the LXe and HPGe detectors at the position used for each measurement. For recoil energies near the extremes of the range of energies for a given configuration, the background from multiple scatter and accidental coincidence events dominates over the recoil peak. The range

of electronic recoil energies over which the scintillation response was calculated was chosen for each data set so that the fraction of events attributable to background in the recoil peak would remain below 20%. To estimate the background contribution in the recoil peak, the event rate in the regions between 2 and 4 σ above and below the peak was computed. This value was then scaled to the width of the peak fitting range and divided by the total event rate in this range. This background contamination estimation method is valid as long as the background varies smoothly in energy, as was observed to be the case in all spectra above recoil energies of 5 keV. Table I lists the resulting ranges over which the scintillation response was calculated for each Compton coincidence data set.

The mean electronic recoil energy does not exactly correspond to E_γ minus the central value of the HPGe energy range selected, because the event rate varies as a function of the recoil energy (see Fig. 2), due to the geometrical acceptance of the detectors. In a region where the event rate increases as a function of recoil energy, for γ-ray scattering angles smaller than the angle at which the HPGe detector is positioned, the mean electronic recoil energy obtained from the HPGe energy selection will be higher than expected since more events at higher recoil energies will be included in the selection. Similarly, the mean electronic recoil energy obtained will be lower than expected in a region where the event rate decreases as a function of recoil energy. The finite energy resolution of the HPGe detector accentuates this effect since even more events from higher or lower energies will be shuffled. The mean and spread of the electronic recoil energy for a given HPGe energy selection was calculated using the simplified Monte Carlo simulation described in Sec. IV B, applying the same energy selection criteria as for the data.

The HPGe energy selection also has an effect on the spatial distribution of events within the LXe detector. Events for which the γ-ray scattering angle is close to θ_{HPGe}, and hence those for which the HPGe energy selection window is close to $E_{\mathrm{er}}(\theta_{\mathrm{HPGe}})$, will be distributed somewhat uniformly in the center of the LXe detector. As the central value of the HPGe energy selection is decreased, however, events will progressively cluster near the side of the LXe detector towards higher scattering angles. Similarly, events will progressively cluster near the side of the LXe detector towards lower scattering angles when the central value of the HPGe energy selection is increased. The relative bias in the measured scintillation response from this effect was estimated using the simplified Monte Carlo simulation and found to be smaller than 0.7%, mostly due to the small spatial variation of the light detection efficiency of the LXe detector [8]. This effect is further suppressed since the energy range over which the scintillation response is calculated is already restricted by limiting the maximum background contamination of the electronic recoil energy peak. Recoil energy ranges corresponding to highly clustered event distributions are thus avoided.

V. SCINTILLATION RESPONSE TO MONOENERGETIC SOURCES

Several radioactive sources were used to evaluate the response of the LXe detector. Specifically, ^{137}Cs, ^{22}Na, and ^{57}Co external sources were used to obtain the γ-ray response of the LXe detector while ^{83m}Kr was used as an internal source for the response to fast electrons.

A. Response to external γ-ray sources

The measurements with external sources were performed by attaching the sources to the cryostat vessel at the height of the LXe active volume. These measurements were taken without the additional $\times$ 10 amplification (Sec. II) of the PMT signal to prevent saturation of the flash ADC, which has a maximum input voltage of 2.25 V. In the normal configuration, saturation starts to occur for signals of 10^3 pe on a single PMT, whereas in this configuration the response from the 1.275 MeV γ ray from ^{22}Na, with a mean signal per PMT of 4.6×10^3 pe, could be measured without any saturation effect.

Figure 5 shows a scintillation spectrum obtained with the ^{137}Cs source. The peak at 16×10^3 pe corresponds to the 661.7 keV full absorption peak while the other peaked feature at 5×10^3 pe is the backscatter peak, mainly due to γ rays that scatter in materials immediately surrounding the LXe active volume before photoelectric absorption in the outer layers of the active volume. The roll-off at low energies is due to the increased effective trigger threshold

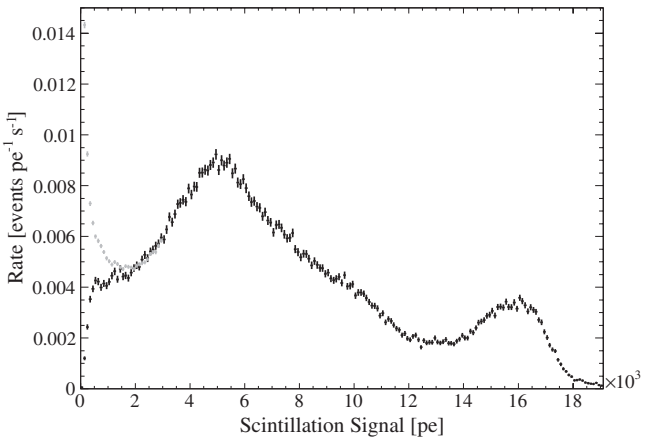

FIG. 5. LXe scintillation spectrum obtained with the 370 MBq ^{137}Cs γ source without (black) and with (gray) additional $\times$ 10 amplification. The peak at 16×10^3 pe corresponds to the 661.7 keV full absorption peak, while the other peaked feature at 5×10^3 pe is mainly due to the backscatter peak. The event rate increase at low energies is visible in the spectrum with additional amplification, as is also observed in the accidental coincidence spectra from the Compton coincidence measurements.

TABLE II. Measured scintillation yields for various external γ-ray sources and for the internal irradiation with ^{83m}Kr.

Source	Energy (keV)	Type	Scintillation Yield (pe/keV)
^{22}Na	1274.6	γ	22.26 ± 0.08(stat) ± 0.77(sys)
^{137}Cs	661.7	γ	23.84 ± 0.08(stat) ± 0.85(sys)
^{22}Na	511	γ	23.76 ± 0.18(stat) ± 1.07(sys)
^{57}Co	122	γ	23.60 ± 0.03(stat) ± 0.85(sys)
^{83m}Kr	32.1	e^-	27.38 ± 0.12(stat) ± 0.82(sys)
^{83m}Kr	9.4	e^-	28.80 ± 0.08(stat) ± 0.86(sys)[a]

[a]This value depends on the time difference between the 32.1 and 9.4 keV transitions, see Sec. VII for details.

when the additional × 10 amplification is not applied to the PMT signals (black points). At low energies, in the spectrum with the additional × 10 amplification, the event rate rises exponentially (gray points). As discussed in Sec. IV A the suspected origin of these events is the small probability for scintillation photons produced outside the active LXe volume to leak into it. This feature at low energies is observed in all spectra obtained with external γ-ray sources.

The large photocathode coverage and the use of PTFE as a scintillation light reflector on the few remaining surfaces assures a good uniformity of the light collection efficiency throughout the active volume. Even so, there is a slight increase in the light collection efficiency near the surface of the PMT windows. The light propagation simulation mentioned in Sec. IV B estimates this increase to be ~6% with respect to the volume-averaged light collection efficiency. This LXe detector spatial nonuniformity can systematically increase the measured scintillation yield of low-energy γ rays from external sources such as ^{57}Co. To mitigate this effect, three cuts on the relative light ratio between two opposing PMTs are applied to the ^{57}Co data to select interactions that occur further from the PMT windows. The volume-averaged scintillation yield obtained at 122 keV is $23.60 \pm 0.03(\text{stat}) \pm 0.85(\text{sys})$ pe/keV, consistent with the value of Ref. [8].

Table II lists the measured scintillation yields for the various external γ-ray sources used to evaluate the scintillation response of the LXe detector. The statistical uncertainty comes from the fit of the spectra and the variation with different fitting ranges on the spectra. The systematic uncertainty includes contributions from the measured variations in the PMT gains and in the response at different source positions.

B. Internal ^{83m}Kr irradiation

The ^{83m}Kr isomer, produced in the decay of ^{83}Rb via pure electron capture, decays to the ground state through two subsequent transitions of 32.1 and 9.4 keV, with half-lives of 1.83 h and 154 ns, respectively. Table III lists the possible deexcitation channels and their branching ratios for the two transitions, as well as the different energies of the electrons emitted in each channel. Branching ratios were obtained from theoretical internal conversion coefficients calculated by the BRICC program [23] and fluorescence yields from Ref. [24]. In both cases, most of the time the energy is carried by internal conversion and Auger electrons.

TABLE III. De-excitation channels and branching ratios of the 32.1 and 9.4 keV transitions of ^{83m}Kr. For both transitions, most of the time the energy is carried by internal conversion electrons (CE) and Auger electrons (A) instead of γ rays. Numbers in parentheses correspond to electron energies in keV.

Transition Energy	Decay Mode	Branching Ratio [%]
32.1 keV	$CE_{M,N}(32)$	11.5
	$CE_L(30.4) + A(1.6)$	63.8
	$CE_K(17.8) + X_{K\alpha}(12.6) + A(1.6)$	15.3
	$CE_K(17.8) + A(10.8) + 2A(1.6)$	9.4
	γ	<0.1
9.4 keV	$CE_L(7.5) + A(1.6)$	81.1
	$CE_M(9.1)$	13.1
	γ	5.8

The use of ^{83m}Kr as a calibration source allows a uniform internal irradiation of the LXe detector, eliminating most of the problems mentioned earlier concerning low-energy calibrations with external γ-ray sources. Additionally, the scintillation signals produced in LXe by the two subsequent ^{83m}Kr transitions can be separated in time and thus provide precise scintillation yield measurements with negligible background contribution [14], even at low source activities. Since the bulk of the energy in the 32.1 keV transition of ^{83m}Kr is most often carried by a 30.4 keV conversion electron, its scintillation response should provide an independent verification of the scintillation yield at that energy obtained in the Compton coincidence measurement. Similarly, the scintillation response of the 9.4 keV transition is expected to be similar to that obtained in the Compton coincidence measurement.

The source used for the irradiation was composed of zeolite beads containing ^{83}Rb, which emanate ^{83m}Kr from ^{83}Rb decays. The ^{83}Rb activity of the source used was 3.45 kBq. The source was located in a stainless steel cylinder connected to the gas system through a 2-μm filter and isolated with a valve. The rate of ^{83m}Kr decays observed was 8 mHz, much lower than the activity of the source. This large reduction in observed rate is attributed to a low efficiency in the convective transport of ^{83m}Kr atoms into the active volume of the LXe detector. The bulk motion of LXe itself in and out of the active volume is limited by the small open area between PMTs and the PTFE holding structure (Sec. II). Nevertheless, the distinctive signature of the two ^{83m}Kr transitions allows a clear selection of these events above background. The measured half-life between the two transitions is 154 ± 6 ns, in agreement with previously measured values [25,26].

Figure 6 shows the measured scintillation spectra for the 9.4 and 32.1 keV transitions. The scintillation response for the 9.4 keV transition is compatible with a Gaussian, whereas the response for the 32.1 keV is not and shows a longer tail at low scintillation values. The 32.1 keV transition is expected, in about 25% of cases, to undergo internal conversion with a K-shell electron, and thus emit a larger number of lower energy electrons than in the case of internal conversion with an L-shell electron (see Table III). If the scintillation yield of electrons were to vary with energy, then the response of the 32.1 keV transition could have two components. Therefore, the response of the 32.1 keV transition is taken as the mean of two Gaussian functions constrained to have the appropriate branching ratios. The scintillation light yield value obtained is $27.38 \pm 0.12(\text{stat}) \pm 0.82(\text{sys})$ pe/keV, with a resolution (σ/E) of 6.9%. The scintillation light yield of the 9.4 keV transition obtained is $28.80 \pm 0.08(\text{stat}) \pm 0.86(\text{sys})$ pe/keV, with a resolution (σ/E) of 11.8%. The measured variation in the PMT gains during the internal irradiation with ^{83m}Kr is taken as the systematic uncertainty in the light yield. The ratio of the measured scintillation light yields of the 32.1 and 9.4 keV decays is 1.052 ± 0.005, a value consistent with the results of Ref. [14], which found 1.056 ± 0.011. In Ref. [15], the scintillation yields measured lead to a slightly lower ratio of 0.976 ± 0.001.

The measured scintillation light yields from the internal irradiation with ^{83m}Kr are summarized in Table II, along with the results for external γ-ray sources.

VI. RESULTS

The precise determination of the absolute scintillation yield requires the precise knowledge of many properties related to the scintillation photon detection probability: the detailed geometry of the active LXe volume, the reflectivity of the materials, and the collection efficiency of the PMTs and their QE (and its possible variation with temperature). Thus, relative yields are reported. The reference chosen is the scintillation yield of the 32.1 keV transition of ^{83m}Kr. The use of a low-energy, uniform, internal source as a reference has major advantages over an external γ-ray source such as ^{57}Co: the systematic uncertainty on the ^{57}Co scintillation yield (Sec. VA) arising from the highly localized event distribution in LXe can be eliminated. Additionally, since the reference source is internal, it readily solves the problem of the small penetration depth of low-energy γ rays in the calibration of the inner volume of large detectors.

The obtained values of the relative scintillation yield of electronic recoils at zero field, $\mathcal{R}_e$, are listed in Table IV. The specific Compton coincidence data sets used to calculate the $\mathcal{R}_e$ values are also listed for each electronic recoil energy, labeled by the scattering angle θ_{HPGe} between the ^{137}Cs source and the center of the LXe and HPGe detectors. Figure 7 shows the results as a function of electronic recoil energy, along with the measured and predicted relative scintillation yields of the 32.1 and 9.4 keV transitions of ^{83m}Kr.

The statistical uncertainty on $\mathcal{R}_e$ comes from the fit of the electronic recoil peak, while the systematic contributions arise from uncertainties in the PMT gains, σ_{g_i}, the HPGe calibration factor, $\sigma_{C_{\text{HPGe}}}$, and the background subtraction, σ_b. The systematic uncertainty arising from the variation in the fitting range and the spread in electronic recoil energies were found to have a negligible impact and

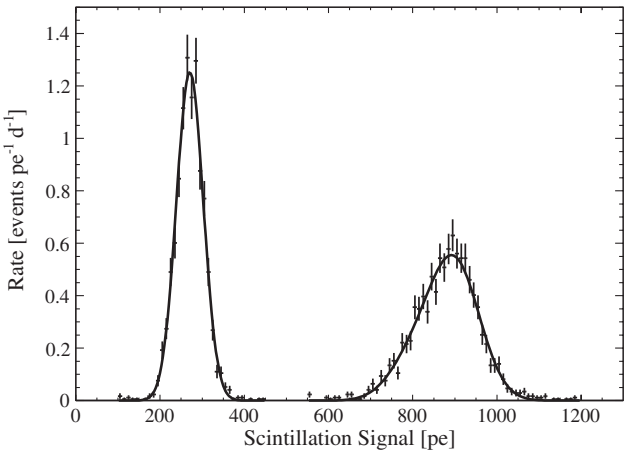

FIG. 6. Measured scintillation spectra (points) for the 9.4 and 32.1 keV deexcitation transitions of ^{83m}Kr, along with their fits (lines). The asymmetry of the scintillation spectrum of the 32.1 keV transition can be explained by a decrease in the response of LXe with decreasing energies.

TABLE IV. Values of the relative scintillation yield of electronic recoils at zero field, $\mathcal{R}_e$, together with their uncertainties, obtained from different sets of Compton coincidence measurements, labelled by the scattering angle θ_{HPGe} between the ^{137}Cs source and the center of the LXe and HPGe detectors.

E_{er} (keV)	Measurements (θ_{HPGe})	$\mathcal{R}_e$
2.1 ± 1.4	0.0°, 5.6°	0.730 ± 0.050
3.2 ± 1.4	0.0°, 5.6°	0.705 ± 0.045
4.3 ± 1.4	0.0°, 5.6°	0.728 ± 0.045
5.8 ± 1.9	0.0°, 5.6°, 8.6°	0.757 ± 0.048
7.3 ± 1.4	0.0°, 5.6°, 8.6°	0.782 ± 0.040
9.3 ± 2.4	0.0°, 5.6°, 8.6°, 12.0°	0.820 ± 0.051
12.3 ± 2.3	0.0°, 5.6°, 8.6°, 12.0°	0.857 ± 0.054
16.3 ± 3.4	0.0°, 5.6°, 8.6°, 12.0°	0.896 ± 0.050
21.3 ± 3.3	0.0°, 8.6°, 12.0°, 16.1°	0.915 ± 0.041
27.8 ± 4.9	0.0°, 8.6°, 12.0°, 16.1°	0.899 ± 0.060
36.2 ± 5.4	16.1°, 21.3°	0.947 ± 0.103
46.7 ± 6.9	21.3°	0.994 ± 0.061
61.1 ± 9.4	21.3°, 28.1°	1.007 ± 0.048
80.2 ± 11.4	21.3°, 28.1°, 34.4°	1.002 ± 0.046
104.2 ± 14.4	28.1°, 34.4°	0.977 ± 0.052
120.2 ± 3.4	34.4°	0.961 ± 0.043

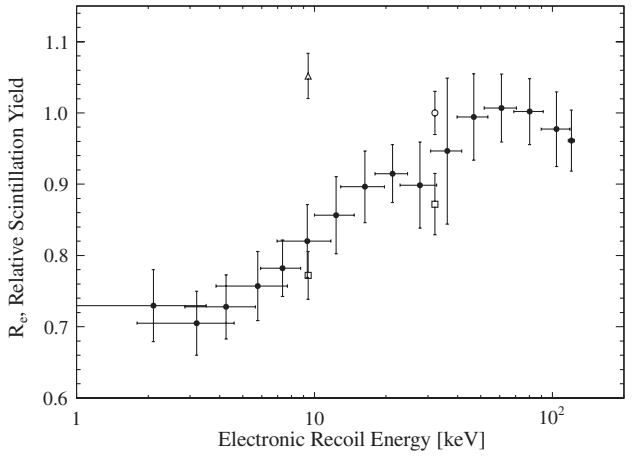

FIG. 7. Measured values (solid circles) of the relative scintillation yield of electronic recoils, $\mathcal{R}_e$, with respect to the scintillation yield of the 32.1 keV transition of ^{83m}Kr (open circle), along with that of the 9.4 keV transition (open triangle). The predicted relative yields of the two transitions, computed from the Compton coincidence results and the electron energies emitted (Table III), are also indicated (open squares). The anomalous scintillation yield of the 9.4 keV transition of ^{83m}Kr, compared to that of an electronic recoil of the same energy, can be understood by the transient state of the LXe after the absorption of the electrons emitted in the 32.1 keV transition, as explained in the text.

are therefore not included. However, the observed variance of $\mathcal{R}_e$ values for the same electronic recoil energy from different measurements was found to be greater than that given by the contributions mentioned above. Consequently, an additional term, $\sigma^2_{\mathcal{R}_e,\mathrm{s}}$, is included in the expression for the total uncertainty on $\mathcal{R}_e$ to account for this. The total uncertainty on $\mathcal{R}_e$ is therefore expressed as

$$\sigma^2_{\mathcal{R}_e} = \sigma^2_{\mathcal{R}_e,\mathrm{fit}} + \sum_i \left(\frac{\partial \mathcal{R}_e}{\partial g_i}\right)^2 \sigma^2_{g_i} + \left(\frac{\Delta \mathcal{R}_e}{\Delta C_{\mathrm{HPGe}}}\right)^2 \sigma^2_{C_{\mathrm{HPGe}}} + \left(\frac{\Delta \mathcal{R}_e}{\Delta b}\right)^2 \sigma^2_b + \sigma^2_{\mathcal{R}_e,s}. \quad (3)$$

The uncertainty in PMT gains is taken as the variation in the measured gains during the data-taking period. The variation in $\mathcal{R}_e$ values with respect to the HPGe detector calibration was calculated through a finite difference approximation, $\Delta\mathcal{R}_e/\Delta C_{\mathrm{HPGe}}$, by repeating the analysis using the calibration factors $C_{\mathrm{HPGe}} \pm \sigma_{C_{\mathrm{HPGe}}}$. For electronic recoil energies below 5 keV ($\theta_{\mathrm{HPGe}} = 0°, 5.6°$), the contribution from the uncertainty in the background subtraction was estimated by repeating the analysis with a different background model. Specifically, since low-energy background events are expected to arise from accidental coincidences between LXe and HPGe detector triggers, as explained in Sec. IV C, an alternate background model based on the energy spectrum of accidental coincidence events was used. LXe scintillation signal and HPGe energy random variates, distributed according to the measured LXe and HPGe detector ^{137}Cs spectra, were used to generate the expected background from accidental coincidence events. The background contamination was calculated such that the resulting LXe scintillation signal spectrum, with the background spectrum subtracted, matched the rate obtained from the GEANT4 Monte Carlo simulation. A recoil energy region virtually free of background, from 10 to 20 keV, was used to normalize the simulated rate.

The additional uncertainty contribution $\sigma^2_{\mathcal{R}_e,\mathrm{s}}$ is taken as a linear function of the recoil energy, from 7.1% at 2 keV down to 3% at 53 keV, and vanishing for recoil energies above 78 keV. For electronic recoil energies below 53 keV, the largest contribution to the uncertainty comes from this additional contribution. The next largest contribution to the uncertainty at these energies comes from the uncertainty in the PMT gains (3%), which is the same for all measurements. At 2 keV, the contribution from the statistical uncertainty (2.8%) and those of the background subtraction (0.8%) and HPGe detector calibration (0.6%) are next in size. At recoil energies above 53 keV, the contribution from the PMT gains dominates while the contributions from other effects are negligible.

When multiple $\mathcal{R}_e$ values were obtained at a given electronic recoil energy from different Compton coincidence data sets, the results were averaged taking the total uncertainty of each value into account. Similarly, values of $\mathcal{R}_e$, which were calculated at 1 keV HPGe energy intervals, were averaged over ranges of electronic recoil energies where $\mathcal{R}_e$ did not vary appreciably.

VII. DISCUSSION

To our knowledge, these results are the first measurements of the scintillation response of LXe to nearly monoenergetic low-energy electrons over a wide range of energies. The Compton coincidence technique allows the production of electronic recoils which most closely resemble the background of large LXe dark matter detectors, without the need to deconvolve the response for any atomic shell effects present in the case of the response to low-energy photoabsorbed γ rays.

Our results suggest that the scintillation yield of electronic recoils at zero field increases as the electron energy decreases from 120 to about 60 keV but then decreases by about 30% from 60 to 2 keV, contrary to the intuition that it should continue to increase with ionization density. This odd behavior is expected, however, since the electron-ion recombination probability has been shown to become independent of ionization density for low-energy electronic recoils [27]. It is also expected since low-energy photoabsorbed γ rays exhibit a decrease in scintillation yield with decreasing energies [28]. For an electronic recoil track size smaller than the electron thermalization length in LXe, an increase in ionization density is not

accompanied by an increase in recombination probability as ionization electrons thermalize in a volume larger than that of the track. In fact, the energy at which the turnover is observed in our measurement corresponds very closely to the energy at which the average electronic recoil track size calculated in Ref. [27] reaches 4.6 μm, the estimated value for the electron thermalization length in LXe [29]. This length scale is also used in the NEST model [28] to bridge the low- and high-energy regime recombination models. At zero field, these electrons either recombine at much longer time scales [10,30,31], attach to impurities, or eventually leave the active volume of the detector, in all cases contributing to the reduction in scintillation light from recombination.

The scintillation yield obtained from the Compton coincidence measurement is compatible with the measured yield of the 32.1 keV transition of ^{83m}Kr, in which the bulk of the energy released, as described in Sec. V B, is most often (75%) carried by a 30 keV internal conversion electron. The scintillation yield of the 9.4 keV transition of ^{83m}Kr, however, is not compatible with the value from the Compton coincidence measurement. Assuredly, such a marked disagreement between the two measured values prompted a search for possible unaccounted systematic effects in one or both measurements. A notable difference between an energetic electron produced in the LXe detector by a γ-ray Compton scatter and a conversion electron from the 9.4 keV transition is that the latter is produced a very short time, 220 ns on average, after another energetic electron, the 30 keV internal conversion electron from the 32.1 keV transition, transferred its energy to the LXe. On that time scale, electrons and positive ions from the track of the 32.1 keV transition conversion electron which have not recombined might still populate the immediate vicinity of the Kr atom. In the context of the Thomas-Imel model [32], in which recombination depends on the number of Xe ions the enhancement in the scintillation yield could be understood as being due to the effective increase in number of ions left over from the previous interaction. The fact that the predicted relative yields of the two transitions (Fig. 7, open squares), computed from the Compton coincidence results and the electron energies emitted (Table III) are both lower than the measurements, is also consistent with the above interpretation. That is, subsequent deexcitations in the cascade have enhanced scintillation yields, compared to those of isolated recoiling electrons of the same energy, since they occur very close in time and in the immediate vicinity of previous tracks.

If the scintillation yield of the 9.4 keV transition of ^{83m}Kr were to decrease with an increasing time difference between the two transitions, this would provide a strong indication that the transient state of the LXe is responsible for the anomalously high scintillation yield of the 9.4 keV transition, compared to that measured for Compton electrons of a similar energy. Figure 8 shows the measured

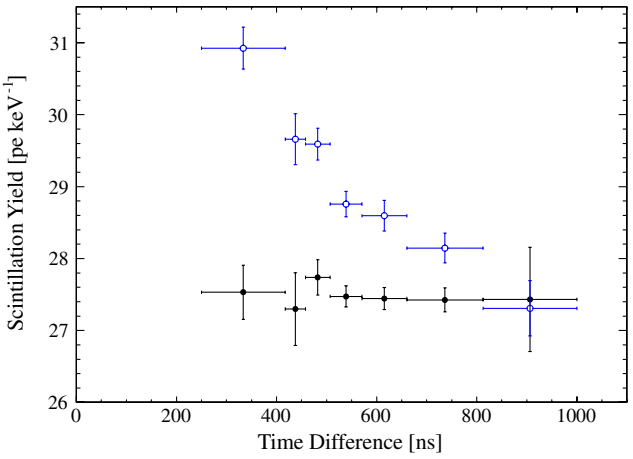

FIG. 8 (color online). Scintillation yields of the 9.4 keV (open blue circles) and 32.1 keV (solid black circles) transitions of ^{83m}Kr as functions of the time difference between the two scintillation signals. While the measured yield of the 32.1 keV transition is constant with increasing time difference, that of the 9.4 keV transition decreases. This is a strong indication that the transient state of the LXe is responsible for the discrepancy observed with respect to the yield measured with the Compton coincidence method at this energy.

scintillation yields for both transitions as a function of the time difference between the two scintillation signals. The scintillation yield of the first transition (32.1 keV) shows no time dependence while that of the second transition (9.4 keV) exhibits a decrease of 12% from time differences of 300–900 ns. This raises doubts on the suitability of ^{83m}Kr as a calibration source in LXe at 9.4 keV, at least at zero electric field.

The efficiency of the data processing software in separating scintillation signals, which themselves have decay times on the order of 45 ns [33] at zero field, from two energy deposits very close in time, such as the two transitions of ^{83m}Kr, necessarily implies a loss in detection efficiency at short time differences. This efficiency loss, likely different for measurements from different groups, coupled to a time-dependent decrease in the scintillation yield of the 9.4 keV transition, could explain the discrepancy between the ratio of scintillation yields of the 9.4 and 32.1 keV transition of ^{83m}Kr of this work and the one in Ref. [15] a quantity which one would otherwise expect to be virtually free of most systematic effects.

We have chosen to report relative instead of absolute yields to eliminate systematic uncertainties in the total light detection efficiency of the LXe detector from the measurement. The precise reason for the very high absolute light yield obtained is not known, although two very likely effects are a temperature dependence of the QE of the PMTs for LXe scintillation light [34], and a change in the effective QE of the PMTs as a function of the angle of an incident photon [22], the latter being a much more pronounced effect for a compact detector such as the one used in this measurement. We have chosen to report our

results relative to the scintillation yield of the 32.1 keV transition of ^{83m}Kr to minimize the uncertainty from any position dependence in the light detection efficiency.

We have shown that the improved Compton coincidence technique [18], with a high energy resolution HPGe detector, can be used to provide a source of electronic recoils with a precise energy and small energy spread (~ 1 keV). This technique allows the measurement of the response of LXe to electrons with energies as low as a few keV and is only limited by the resolution of the HPGe detector near the Compton scattered γ-ray energy.

ACKNOWLEDGMENTS

This work was carried out with support from the National Science Foundation for the XENON100 Dark Matter experiment at Columbia University (Grant No. PHYS09-04220).

[1] E. Aprile *et al.* (XENON100), Phys. Rev. Lett. **105**, 131302 (2010).
[2] E. Aprile *et al.* (XENON100), Phys. Rev. Lett. **107**, 131302 (2011).
[3] E. Aprile *et al.* (XENON100), Phys. Rev. Lett. **109**, 181301 (2012).
[4] E. Aprile *et al.* (XENON), in *Proceedings of UCLA DM 2012* (to be published).
[5] E. Aprile *et al.* (XENON100), Astropart. Phys. **35**, 573 (2012).
[6] E. Aprile, K. Giboni, P. Majewski, K. Ni, M. Yamashita, R. Hasty, A. Manzur, and D. McKinsey, Phys. Rev. D **72**, 072006 (2005).
[7] E. Aprile, L. Baudis, B. Choi, K. L. Giboni, K. Lim, A. Manalaysay, M. E. Monzani, G. Plante, R. Santorelli, and M. Yamashita, Phys. Rev. C **79**, 045807 (2009).
[8] G. Plante, E. Aprile, R. Budnik, B. Choi, K.-L. Giboni, L. W. Goetzke, R. F. Lang, K. E. Lim, and A. J. Melgarejo Fernandez, Phys. Rev. C **84**, 045805 (2011).
[9] T. Doke, A. Hitachi, J. Kikuchi, K. Masuda, H. Okada, and E. Shibamura, Jpn. J. Appl. Phys. **41**, 1538 (2002).
[10] T. Doke, H. J. Crawford, A. Hitachi, J. Kikuchi, P. J. Lindstrom, K. Masuda, E. Shibamura, and T. Takahashi, Nucl. Instrum. Methods Phys. Res., Sect. A **269**, 291 (1988).
[11] I. R. Barabanov, V. N. Gavrin, and A. M. Pshukov, Nucl. Instrum. Methods Phys. Res., Sect. A **254**, 355 (1987).
[12] I. M. Obodovskii and K. T. Ospanov, Instrum. Exp. Tech. **37**, 42 (1994).
[13] M. Yamashita, T. Doke, K. Kawasaki, J. Kikuchi, and S. Suzuki, Nucl. Instrum. Methods Phys. Res., Sect. A **535**, 692 (2004).
[14] A. Manalaysay *et al.*, Rev. Sci. Instrum. **81**, 073303 (2010).
[15] L. Kastens, S. Cahn, A. Manzur, and D. McKinsey, Phys. Rev. C **80**, 045809 (2009).
[16] J. Valentine and B. Rooney, Nucl. Instrum. Methods Phys. Res., Sect. A **353**, 37 (1994).
[17] B. Rooney and J. Valentine, IEEE Trans. Nucl. Sci. **43**, 1271 (1996).
[18] W.-S. Choong, K. M. Vetter, W. W. Moses, G. Hull, S. A. Payne, N. J. Cherepy, and J. D. Valentine, IEEE Trans. Nucl. Sci. **55**, 1753 (2008).
[19] J. Jortner, L. Meyer, S. A. Rice, and E. G. Wilson, J. Chem. Phys. **42**, 4250 (1965).
[20] K. L. Giboni, E. Aprile, B. Choi, T. Haruyama, R. F. Lang, K. E. Lim, A. J. Melgarejo, and G. Plante, J. Instrum. **6**, P03002 (2011).
[21] S. Agostinelli *et al.* (GEANT4), Nucl. Instrum. Methods Phys. Res., Sect. A **506**, 250 (2003).
[22] *Hamamatsu Photonics K.K., Photomultiplier Tubes: Basics and Applications* (Hamamatsu Photonics K.K., Hamamatsu, 2006), 3rd ed., http://sales.hamamatsu.com/assets/applications/ETD/pmt_handbook_complete.pdf.
[23] T. Kibedi, T. W. Burrows, M. B. Trzhaskovskayac, P. M. Davidsona, and C. W. Nestor Jr., Nucl. Instrum. Methods Phys. Res., Sect. A **589**, 202 (2008).
[24] J. H. Hubbell, P. N. Trehan, N. Singh, B. Chand, D. Mehta, M. L. Garg, R. R. Garg, S. Singh, and S. Puri, J. Phys. Chem. Ref. Data **23**, 339 (1994).
[25] I. Ahmad, K. E. Rehm, E. P. Kanter, W. Kutschera, W. R. Phillips, and A. R. Barnett, Phys. Rev. C **52**, 2240 (1995).
[26] S. L. Ruby, Y. Hazoni, and M. Pasternak, Phys. Rev. **129**, 826 (1963).
[27] C. E. Dahl, Ph.D. thesis, Princeton University, 2009.
[28] M. Szydagis, N. Barry, K. Kazkaz, J. Mock, D. Stolp, M. Sweany, M. Tripathi, S. Uvarov, N. Walsh, and M Woods, JINST **6**, P10002 (2011).
[29] A. Mozumder, Chem. Phys. Lett. **245**, 359 (1995).
[30] S. Kubota, A. Nakamoto, T. Takahashi, T. Hamada, E. Shibamura, M. Miyajima, K. Masuda, and T. Doke, Phys. Rev. B **17**, 2762 (1978).
[31] S. Kubota, M. Hishida, M. Suzuki, and J.-z. Ruan(Gen), Phys. Rev. B **20**, 3486 (1979).
[32] J. Thomas and D. Imel, Phys. Rev. A **36**, 614 (1987).
[33] A. Hitachi, T. Takahashi, N. Funayama, K. Masuda, J. Kikuchi, and T. Doke, Phys. Rev. B **27**, 5279 (1983).
[34] E. Aprile, M. Beck, K. Bokeloh, R. Budnik, B. Choi *et al.*, J. Instrum. **7**, P10005 (2012).